

## Supporting information

### Excellent Microwave Absorption Property of

### *h*-BN-GO-Fe<sub>3</sub>O<sub>4</sub> Ternary Composite

Hua Pang,<sup>a</sup>\*Wenhui Pang<sup>a</sup>, Bo Zhang<sup>b</sup>, and Nan Ren<sup>c</sup>,

\*Corresponding authors

E-mail addresses: [hpang@lzu.edu.cn](mailto:hpang@lzu.edu.cn)

School of Physical Science and Technology, Lanzhou University, Lanzhou 730000, China

Key Laboratory for Magnetism and Magnetic Materials of the Ministry of Education, Lanzhou 730000, China

#### SEM images

From the SEM image of GO (Fig.S1 (a)), it can be seen that layered GO resembles crumpled silk veil. The XRD pattern of GO (Fig.S1 (b)) reveals an intense and sharp peak centered at  $2\theta=11.5^\circ$ , corresponding to the (001) interplanar spacing of 0.8 nm. For GO-Fe<sub>3</sub>O<sub>4</sub> (Fig.S1 (c) and (d)), disordered Fe<sub>3</sub>O<sub>4</sub> microplates form a layered stacking structure. Fig.S1 (e) and (f) shows the microscopic morphology of *h*-BN-Fe<sub>3</sub>O<sub>4</sub> composite, the *h*-BN nanoplates disperse randomly and aggregate slightly.

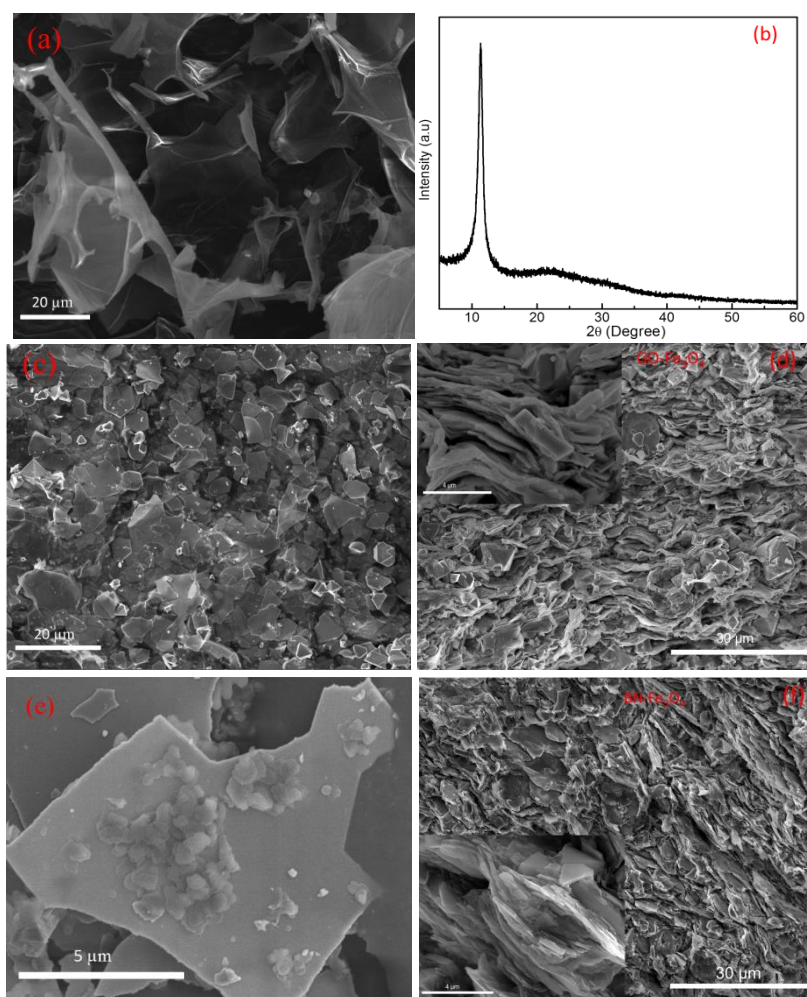


Fig.S1 (a) and (b) the SEM image and XRD pattern of GO; (c) and (d) the microstructures GO-Fe<sub>3</sub>O<sub>4</sub> composite; (e) and (f) the microstructures of *h*-BN-Fe<sub>3</sub>O<sub>4</sub> composites.

### Element mapping

Fig.S2 shows a typical SEM image of the *h*-BN-GO-Fe<sub>3</sub>O<sub>4</sub> composite, together with the elemental mapping of Fe, O, C, B and N. The uniform distribution of Fe and O confirms that the microplates are Fe<sub>3</sub>O<sub>4</sub> particles. The distribution of element C in the particle region is uniform, indicating that GO dispersed on the surface of the Fe<sub>3</sub>O<sub>4</sub> particles. The strengthened intensity of element C outside the microplates region is ascribed to the contribution of the carbon adhesive. Moreover, the distribution of B and N is uneven and shows local agglomeration, suggesting the *h*-BN particles distributed randomly and segregated slightly on the Fe<sub>3</sub>O<sub>4</sub> particles.

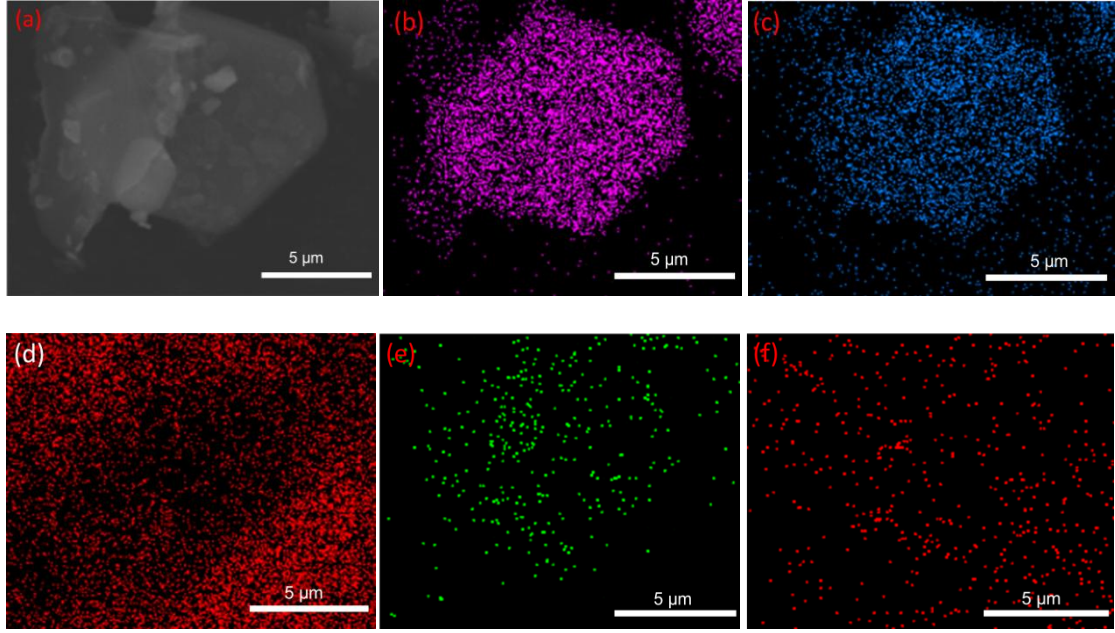


Fig.S2 Typical SEM image of *h*-BN-GO-Fe<sub>3</sub>O<sub>4</sub> and elemental mapping of Fe, O, C, N and B.

### Microwave EM properties

The frequency dependences of the complex permeability  $\mu_r$  and complex permittivity  $\varepsilon_r$  of Fe<sub>3</sub>O<sub>4</sub> and GO samples are shown in Fig. S3. The Fe<sub>3</sub>O<sub>4</sub> sample shows much higher  $\varepsilon_r$  value compared with the corresponding  $\mu_r$  value in the range of 1.0-18.0 (Fig.S3 (a) and (b)). The  $\mu'$  value of the Fe<sub>3</sub>O<sub>4</sub> sample reduced from 2.5 to 0.72 while the  $\mu''$  value remained between 0.9-1.2 in the frequency range of 1.0-8.0 GHz, afterwards both parameters decrease rapidly. The large values of  $\mu''$  and the broad peak in the  $\mu'' \sim f$  curve in the frequency range of 1.0-8.0 GHz indicate an enhanced magnetic loss and evaluated resonance frequency of Fe<sub>3</sub>O<sub>4</sub> microplates.

Fig.S3 (c) shows the frequency dependences of  $\mu''(\mu')^{-2} f^{-1}$  and  $tg\delta_\mu$  for the Fe<sub>3</sub>O<sub>4</sub>.

As can be seen, the  $\mu''(\mu')^{-2} f^{-1}$  values at different frequencies are close to each other ( $\approx 0.11$ ) over 2.2–7.2 GHz, indicating that the magnetic loss is mainly caused by the eddy current effect in this band region. After that the frequency dependence of  $\mu''(\mu')^{-2} f^{-1}$  is distinct, especially around 8.2-10.0 GHz where  $tg\delta_\mu$  manifests a broad peak, which means the magnetic loss should be ascribed the nature resonance then.

For GO sample, as shown in Fig.S3 (d) to (f), the real permittivity  $\varepsilon'$  decreases from 12.4 at 1 GHz to 6.4 at 18 GHz, whereas the imaginary permittivity  $\varepsilon''$  drops from 6.4 at 1 GHz to 2.5 at 18 GHz. The dielectric loss tangent  $tg\delta_\varepsilon$  of GO is the

highest of all materials, which is above 0.4 in the frequency range of 4.0 - 18.0 GHz.

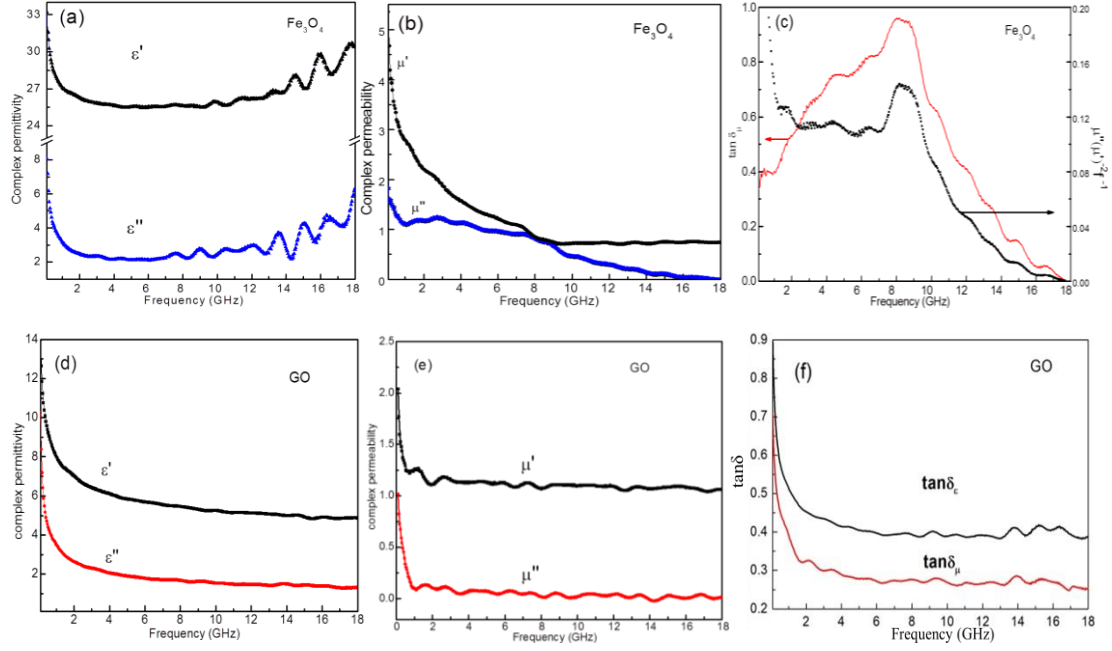


Fig.S3 (a) and (b) complex permittivity ( $\epsilon'$  and  $\epsilon''$ ) and permeability ( $\mu'$  and  $\mu''$ ) of  $\text{Fe}_3\text{O}_4$ , (c) magnetic loss tangent and the frequency dependences of  $\mu''/(\mu')^2 f^{-1}$  for  $\text{Fe}_3\text{O}_4$ ; (d) and (e) complex permittivity ( $\epsilon'$  and  $\epsilon''$ ) and permeability ( $\mu'$  and  $\mu''$ ) of GO, (f) dielectric and magnetic loss tangent of GO.

### Calculations of effective permittivity

To explore the role of interlayer voids in modifying the effective permittivity of the materials, we analysis the experimental values of  $h\text{-BN-Fe}_3\text{O}_4$  and  $h\text{-BN-GO-Fe}_3\text{O}_4$  samples based on effective medium theory. Here the Lichtenecker's

law is adopted, <sup>1</sup> as  $\epsilon_{\text{eff}} = \prod_{i=1}^N \epsilon_i^{f_i}$ , where  $\epsilon_i$  and  $f_i$  are the relative permittivity and

volume fraction of component  $i$  in the composite. The Lichtenecker's law can be deduced directly from Maxwell equations and provides good estimate of the effective dielectric properties of artificial heterogeneous composites with a wide range of surface fractions. <sup>2, 3</sup> In the calculations, the volume ratio of each component is obtained according to the mass ratio in the composites. The complex permittivity of  $\text{Fe}_3\text{O}_4$  and GO come from the experimental measurements while the values reported in the literatures are adopted for  $h\text{-BN}$  <sup>4</sup> and paraffin <sup>5</sup> since they are quite stable in the experimental frequency range.

In Fig.S4 we show the calculation results using Lichtenecker's law (solid lines) and the experimental results (lines plus open circles) of the complex permittivity of

$h$ -BN-Fe<sub>3</sub>O<sub>4</sub> and  $h$ -BN-GO-Fe<sub>3</sub>O<sub>4</sub> composites. For the ternary composite sample (Fig.S4 (a)), the calculated effective permittivity is much larger than the experimental value during the whole frequency range without considering the contribution of voids. When taken the voids as the fourth component, the fitting result is greatly improved. Best fitting yields the volume fraction of the voids about ~20% when fix the relative volume ratio of the three components. This indicates that the voids can reduce the complex permittivity of the ternary composite sample effectively. The discrepancy between the measured and calculated values of  $\epsilon_r$  can be attributed to the simplicity of the theoretic model and the uncertainty in the evaluation of the intrinsic permittivity of the components.

For  $h$ -BN-Fe<sub>3</sub>O<sub>4</sub> (Fig.S4 (b)), satisfactory fitting results can be obtained without considering the air phase, and addition of voids contributions will make the calculated values smaller than the experimental values. This observation excludes the possibility of considerable volume fraction of voids, matching with the BET measurement.

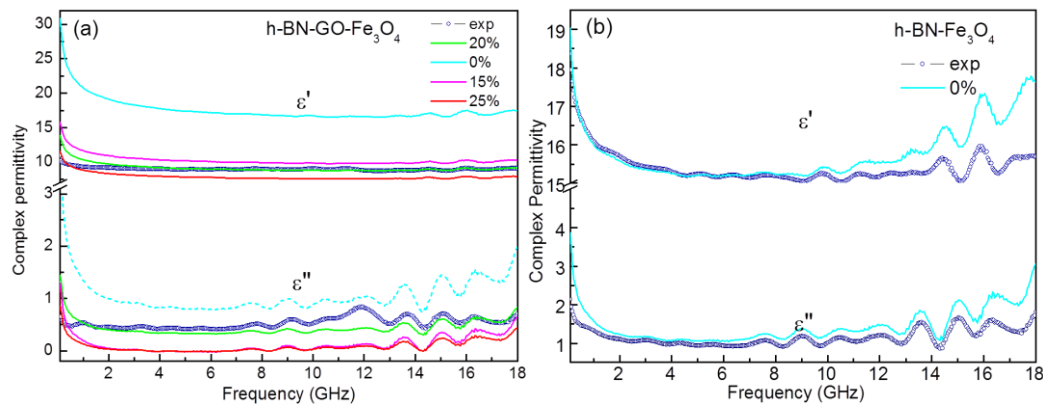


Fig.S4 The real part,  $\epsilon'$ , and the imaginary part,  $\epsilon''$ , of the complex permittivity as a function of frequency for  $h$ -BN-GO-Fe<sub>3</sub>O<sub>4</sub> (a) and  $h$ -BN-Fe<sub>3</sub>O<sub>4</sub> (b). The experiments are denoted by line and open circles. The solid curves are calculations using Lichtenecker's law at different volume fraction of voids.

## References

1. R.Simpkin. Derivation of lichtenecker's logarithmic mixture formula from maxwell's equations. *IEEE Transactions on Microwave Theory & Techniques*, 2010, **58**, 545-550.
2. T. Zakri. Time domain reflectometry techniques for water content measurement. *High Temp. -High Pressure*, 1998, **30**, 19-23.
3. Bouazzaoui S E and Achour M E, Brosseau C. Microwave effective permittivity of carbon black filled polymers: Comparison of mixing law and effective medium equation predictions. *Journal of Applied Physics*, 2011, **110**, 1277-227.
4. Ghassemiparvin, Behnam and N. Ghalichechian. Permittivity and dielectric loss measurement

of paraffin films for mmW and THz applications. *International Workshop on Antenna Technology IEEE*, 2016, 48-50.

5. Baeraky and Thoria, A..Determination of microwave electrical characteristics of boron nitride at high temperature. *Physica Status Solidi*, 2010, **2**, 2577-2580.